Materials Research. 2024; 27:e20230445
DOI: https://doi.org/10.1590/1980-5373-MR-2023-0445

Investigating Non-Thermal Plasma-Induced Precipitation in Hypersaline Waters

C. Alves-Junior[a,b], T. F. Melo[a], L. F. A. Almada[a], K. E. S. Fontes[a], J. O. Vitoriano[b], R. S. Pessoa[c], N. A. Debacher[d]*

[a]*Universidade Federal Rural do Semí-árido, Programa de pós-graduação em Ciência e Engenharia de Materiais, Av. Francisco Mota, 572, Bairro Costa e Silva, 59625-900, Mossoró, RN, Brasil.*
[b]*Universidade Federal do Rio Grande do Norte, Programa de Pós-graduação em Engenharia Mecânica, 59078-970, Natal, RN, Brasil.*
[c]*Instituto Tecnológico de Aeronáutica, Laboratório de Plasmas e Processos, 12228-900, São José dos Campos, SP, Brasil.*
[d]*Universidade Federal de Santa Catarina, Departamento de Química, 88040-900, Florianópolis, SC, Brasil.*

Received: October 11, 2023; Revised: April 21, 2024; Accepted: June 21, 2024

In the present study, non-thermal plasma (NTP) of dielectric barrier discharge (DBD) was used to investigate the precipitation of salt from hypersaline waters obtained by evaporating seawater. A dripper was used to release drops of water over the NTP discharge between the droplet surface and a copper ring in a glass tub working as a DBD. Results showed that the precipitation rate of the NTP-treated solution was significantly higher than that of the untreated solution, with a larger number of small crystals formed, and multiple charged ions preferentially precipitated. These findings suggest that the external electric field from NTP aligns and weakens the hydration of ions, leading to the binding of dehydrated cations and anions, and inducing nucleation/precipitation. Additionally, the NTP discharge channels formed at the gas-liquid interface cause rapid dehydration of ions, which further induce nucleation and crystal formation. This could explain the preferential precipitation of small crystals containing multiple charged ions. Overall, the results demonstrate that NTP-DBD is a promising approach for efficient precipitation of salts from hypersaline waters.

Keywords: *Non-thermal plasma, DBD, hypersaline waters, precipitation, ion extraction.*

1. Introduction

Both the solar salt industry and desalination plants produce hypersaline waters with salt concentrations approximately 3.5% w/v greater than seawater. These waters contain a high concentration of different ions such as, Na^+, Cl^-, Mg^{2+}, SO_4^{2-}, and K^+ which can be potentially harmful to the environment[1]. Therefore, techniques of purification/separation of particular interest are those that do not generate waste, such as preferential salt separation and membrane nanofiltration[2-4].

In recent years, non-thermal plasma (NTP) technologies at atmospheric pressure have been used for liquid processing, including nanomaterial processing, plasma sterilization, analytical water chemistry, food preservation, agricultural processing, and water purification[5-7]. NTP is usually generated by an electrical discharge in which high-energy electrons are selectively "pumped", giving them a much higher temperature than heavy particles[8]. Different types of pulsed discharge systems such as dielectric barrier discharge (DBD), corona discharge, gliding arc, and atmospheric pressure plasma jets are used in these applications, with DBD being the most used[9].

For water purification, interesting results found in the literature include the removal of perfluoroalkyl acids[10], plasma-activated water[11], saline water ion extraction[12], and generation of plasma-activated desalinated water[13]. Despite this, much research has been conducted to understand the complexity of the physicochemical processes in plasma-liquid interaction[14].

When plasma species interact with water molecules and solvated salt ions from saline solutions, they induce the formation of different chemical species, including reactive oxygen and nitrogen species, as well as induce the nucleation and precipitation of salt crystals[13,15,16]. Shirai et al.[17] observed intense yellow-light emission from a NaCl electrolyte solution owing to electron bombardment from the plasma discharge. Additionally, El-Tayeb et al.[18] observed a small amount of Cl_2 gas generated when aqueous solutions of $AlCl_3$ and $CaCl_2$ were exposed to NTP. These observations must be considered when saline solutions are exposed to NTP. However, separating the effects due to the action of an electric field or the plasma generated by it is not an easy task. It is known that the process of dissociation and ionization under air-NTP occurs mainly in the liquid-gas interface and the most common reactive oxygen species (ROS) formed by air-NTP in an aqueous medium are •OH, H_2O_2, O• and O_3. In addition, nitrogen-NTP produces nitrite species such as •NO_2, NO•, NO_2, and NO_3^-, which lower the pH and form the strong oxidant peroxynitrite anion, $ONOO^-$, in water. Consequently, the initial characteristics of the liquid, such as the pH, conductivity, and oxy-reduction potential

*e-mail: clodomiro.jr@ufersa.edu.br

(ORP), will be modified during plasma treatment, which may influence the salt precipitation kinetics[19]. On the other hand, experimental evidence demonstrates that electrothermal effects can occur during the ignition of a corona plasma in saline water, resulting in accelerated evaporation, about 3 times faster than control samples[20-22]. It has also been observed that static electric fields can dehydrate ions. It was demonstrated, using electrophoresis, that electric fields in the range of 300 V/cm can dehydrate calcium and potassium ions, while values above 400 V/cm are able to dehydrate magnesium ions[23,24]. Using molecular dynamics simulation for a saline solution, Kadota et al.[25] found an electric field value equal to 2.5 x 10^5 kV/m for sodium dehydration, that is, 4 orders of magnitude higher than the dehydration data for Ca, K and Mg ions of salts determined in the literature. In previous works[15,16], the authors observed an increase in the precipitation of salts from hypersaline waters exposed to NTP of corona discharge, when compared to natural evaporation. It is possible that factors such as changes in the physicochemical properties of the solution (pH, conductivity, and chemical composition), localized heating produced by the NTP discharge channels, and/or ion dehydration by electromagnetic fields, could influence the plasma-enhanced precipitation process. More studies are still needed to better understand this mechanism and how to develop strategies to separate the origin of the phenomenon.

This study investigates the precipitation of salts from hypersaline solutions using NTP produced by DBD, utilizing natural seawater to reflect real-world conditions in the solar salt industry. Two specific samples, S1 and S2, prepared from evaporated seawater, are pivotal in our research: S1 marks the beginning of NaCl precipitation, while S2 is the point at which $MgCl_2$ precipitation commences, impacting the purity of the precipitate. These stages were specifically chosen to simulate the inherent variability and operational challenges faced by the industry. The use of DBD in this context is particularly advantageous due to its selective extraction of high-energy electrons and minimal transfer of thermal energy to the solution, providing new insights that enhance our understanding of these complex physicochemical processes.

2. Materials and Methods

In this study, two samples, S1 and S2, with different levels of total dissolved solids (TDS) were prepared from evaporated seawater to closely simulate the stages of solar salt production (Table 1). S1 corresponds to the initial stage of NaCl precipitation, indicated by a seawater pH of 8.05 and an electrical conductivity of 220.2 mS/cm. As evaporation continues, the salt concentration increases, leading to higher salinity and the commencement of $MgCl_2$ precipitation at S2, which is characterized by a pH of 7.63 and an electrical conductivity of 236.6 mS/cm. These stages are critical as they represent the points at which the purity of the precipitate begins to decrease. The selection of these specific samples reflects the inherent variability of natural seawater and provides a realistic simulation of the operational conditions faced within the solar salt industry. This methodological choice is not only about replicating real-world conditions but also about providing insights that could help optimize processes under the environmental conditions typically absent from controlled laboratory experiments. Each sample was meticulously characterized for density, electrical conductivity, salinity, and chemical composition, with density measurements conducted using a 25 mL pycnometer and electrical conductivity measured using a Hanna waterproof portable EC/Resistivity/TDS/NaCl meter, model HI98192. By aligning our experimental setup with industry standards, we ensure that our findings have practical applicability and contribute to a deeper understanding of the physicochemical dynamics at play in natural seawater evaporation.

The content of dissolved salts in the S1 and S2 samples was determined by dividing the mass of the precipitated salt by the total mass of a 10 mL aliquot after complete evaporation in an oven at 60°C. The two solutions, S1 and S2, were stored in a refrigerator for further study of precipitation with or without plasma exposure. To prevent precipitation, the solutions were agitated before the analysis to ensure redissolution.

For plasma treatment, a device consisting of a dripper was used, releasing drops with a volume of 50 μL at a continuous flow adjusted to 1 drop/s (Figure 1). A stainless-steel needle with a diameter of 1.7 mm was fixed inside a glass tube with an inner diameter of 10 mm and a thickness of 1 mm, was used as the dripper. The upper end of the needle was connected to a 100 mL burette filled with the solution, and the tip was located 10 mm from the end of the glass tube. A copper ring was placed outside the glass tube at 10 mm from its end. The needle in contact with the drop was grounded and the copper ring was connected to a high voltage source. NTP was generated between the droplet surface and copper ring with a glass tube working as a DBD. The NTP power source was a pulsed high-voltage DC device, operating at an average voltage of 11.5 kV and a pulse frequency of 450 Hz, adjusted through a Keysight digital oscilloscope, model DSO-X 2022-A. The pH, temperature and electrical conductivity of the solutions were measured before and after the dripping.

Sample drops were collected, as shown in Figure 1, under vacuum over a qualitative filter paper, using a 90 mm diameter Buchner funnel and a 500 mL Kitasato

Table 1. Characterization of the S1 and S2 starting samples obtained by evaporation of seawater.

Sample	pH	EC mS/cm	Density (g/cm^3)	Ion concentration (g/L)					
				Na^+	K^+	Mg^{2+}	Ca^{2+}	Cl^-	SO_4^{2-}
S1	8.05	220.2	1.220	58.6	2.28	7.30	0.95	81.4	4.27
S2	7.63	236.6	1.248	68.4	3.04	9.36	1.10	101.0	5.12

Each value represents the average of three replicates.

flask (Nevoni vacuum aspirator pump, model 5005. All experiments were performed in triplicate under the same experimental conditions.

After dripping 100 mL of solutions S1 and S2, which correspond to 2000 drops of 50 µL the filter paper was dried at 60°C for 6 h, and the precipitate was removed with a stainless-steel spatula and weighed. The precipitates that could not be removed by the spatula were weighed by subtracting the weight of the dry filter paper from that before dripping. Since this difference did not exceed 5% of the mass removed by the spatula, both for the plasma-treated and untreated samples, it was preferred to disregard this residual portion.

Before each experiment, drops with or without plasma treatment were collected on microscope slides (Figure 2) for analysis of the nucleation/crystallization dynamics using a stereoscopic optical microscope (Nikon, mod; MSZ 18) and a scanning electron microscope (Tescan, model Vega 3). Furthermore, an X-ray diffractometer (Shimadzu, model XRD 6000) was used to characterize the crystalline phases of the precipitate salt.

Thermal images and optical emission spectra analysis were conducted simultaneously using a thermal camera (Flir One Pro-Android) and a UV-VIS optical emission spectrometer (OES) (Ocean Optics USB 4000) with a resolution of 0.1 to 10 nm. The optical spectrometer was coupled with a Toshiba TCD1304AP detector in the wavelength range of 200 to 1000 nm. An optical fiber was positioned inside the tube pointing toward the discharge region between the electrodes to capture the emission spectra of the ionized species produced by the NTP discharge (see Figure 2).

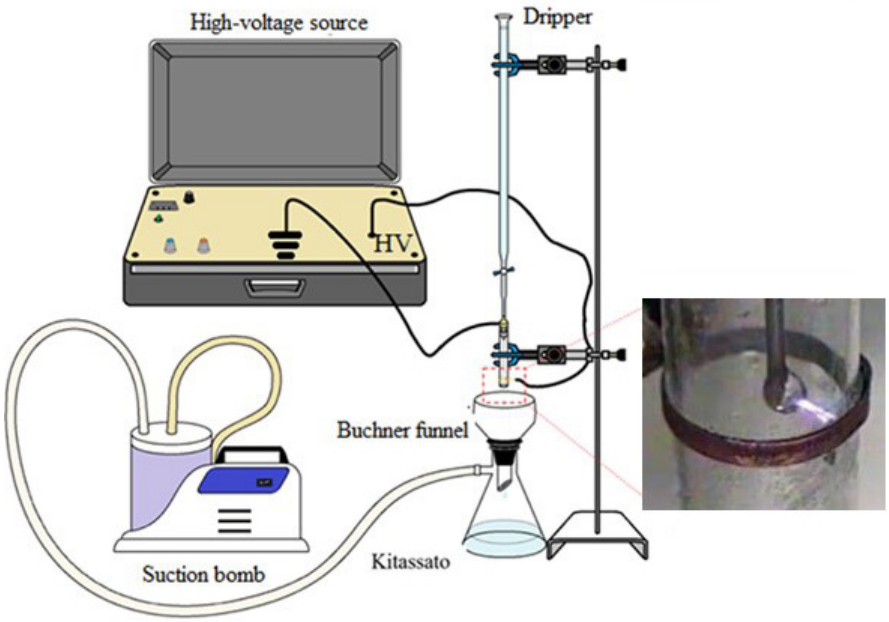

Figure 1. Experimental setup for dripping saline solution, and a detail of the droplet subjected to electrical discharge.

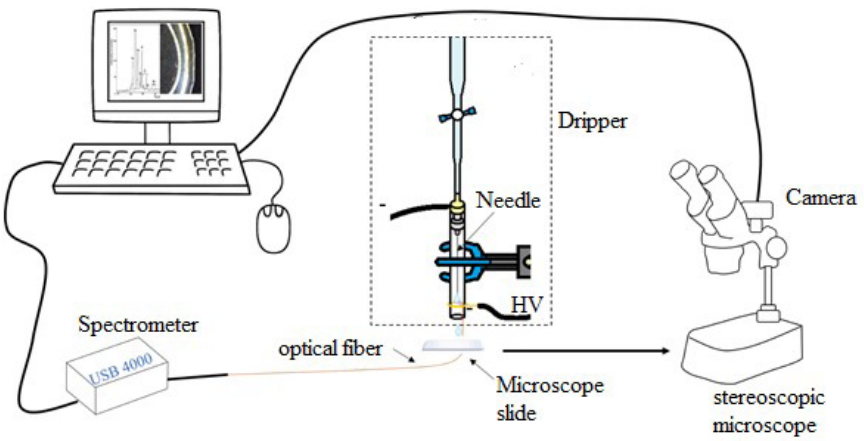

Figure 2. Experimental procedures for analyzing precipitation dynamics using stereoscopic optical and scanning electron microscopies.

The ionic concentrations of sodium and potassium were determined using a Digimed flame photometer, model DM-62, NBR 13806 and 13805). The sulfate ion concentration was measured using optical absorption spectroscopy, employing the turbidimetric method on a UV-VIS spectrophotometer, model Genesys 10S (for Chemical Analysis of Water and Wastes, 1974). The concentration of Cl^-, Ca^{2+} and Mg^{2+} ions were determined using the Mohr method (NBR 13797) and complexometric titration (NBR, 13799 and 12621). The Mg^{2+} concentration was calculated by subtracting the Ca^{2+} ion concentration from the total water hardness. The titrant used for determining hardness consisted of a 0.001M and 0.1M EDTA solution for salt samples and solutions, respectively[26]. The results of chemical and physical analyses of the samples represent the average of three replicates for each condition.

3. Results and Discussion

3.1. Total mass of precipitates

Figure 3 shows the average of three repeated measurements of the precipitated salt mass retained on the filter after dripping, for samples S1 and S2, both exposed and unexposed to the NTP. As shown in Figure 3, the plasma had a significant impact on salt precipitation, increasing by 18.7% for S1 sample and 21.9% for the S2 sample compared to the precipitated mass of the untreated solution. The natural evaporation of a saline solution is a complex phenomenon and depends on several factors, such as relative humidity, temperature, salt mass concentration, and the area of the solution surface[27,28]. Several authors have studied the evaporation of saline droplets, both sessile and pendant, subject to diverse thermal sources[29-31]. In general, the evaporation rate in micro-droplets is higher than that on macroscopic surfaces, being up to 200 times higher for pure water[22]. In a systematic study of pendant salt droplet evaporation, Qu et al.[24] observed that the evaporation rate was constant for different moistures, temperatures, and salinities of the solution.

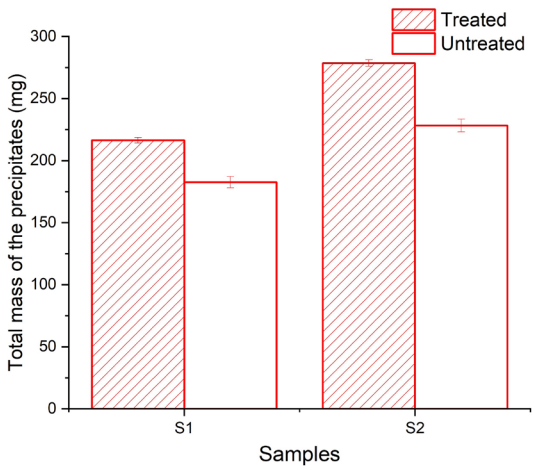

Figure 3. Total mass of precipitates retained on the filter during dripping of 100 mL of S1 and S2 samples, with or without plasma treatment.

Figure 4A shows a free-falling droplet from a height of 50 mm inside the DBD glass tube. Considering the video images from our experiment and the fact that the droplet experiences a free fall, the time of exposure of the droplet to the plasma should not exceed 10 ms. That is, each droplet will experience a maximum of four discharges. The energy consumed in the plasma production process (E_p), employing the Lissajous method[32] to the 100 mL of solution is given by Equation 1:

$$E_p = N_g \int_0^{0.01} V(t)\, dQ(t) \tag{1}$$

where, N_g is the number of drops, $V(t)$ is the discharge voltage, and dQ is the accumulated charge on capacitor C (Figure 4A). The area under the curve for a single pulse is equal to 0.9 mJ, calculated numerically using the curve charge on capacitor vs voltage (Figure 4B), obtained from discharge voltage and current waveforms of the DBD plasma (Figure 4C), and N_g corresponds to 2000 drops of 50 µL.

Thus, if each droplet is subjected to four pulses, the energy transferred by the plasma (E_p) during the dripping of the 2000 drops was equal to 7.2 J, which is much lower than that reported in the literature for the heat of vaporization of water, which is 2.3 x 10^3 kJ/kg[26]. Therefore, the data obtained from Equation 1 shows that evaporation is not the main cause of increased salt precipitation after NTP exposure,

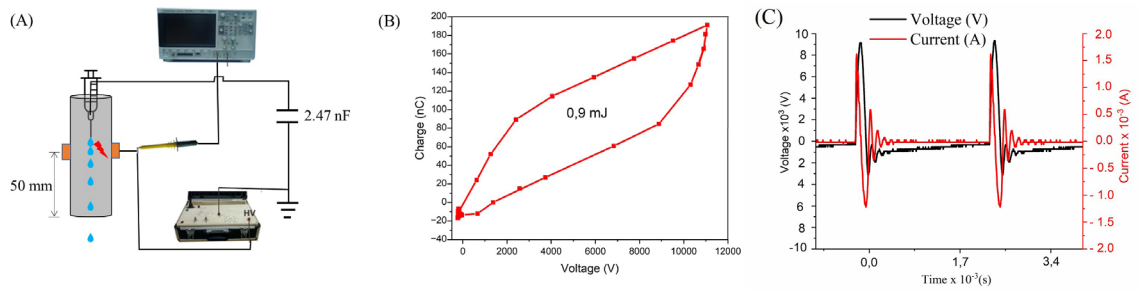

Figure 4. Schematic of measurements of voltage and charge to construct the Lissajous curve during discharge on a free-falling droplet from a height of 50 mm inside the DBD glass tube (A), Curve charge on capacitor vs voltage discharge (B), and voltage current waveforms of the DBD plasma (C).

and there must be other factors involved. Several authors have discussed the effect of an external electric field on the hydration shell for ions in solution[27-29]. When a strong electric field (higher than 10^5 kV/m) interacts with water molecules polarized around an ion, its first hydration layer is weakened, reducing the ion-water interaction energy[29] and, inducing nucleation/crystallization and precipitation. For the voltage used in the present study, 11.5 kV, the electric field generated between the droplet and the electrode (< 1 mm) was around 10^5 kV/m, enough to weaken the bond of salt ions in the first hydration layer.

Furthermore, the electric field induced alignment of water dipoles may lead to nucleation and crystallization when the external electric field competes with the field of individual ions. Consequently, under NTP exposure, dipole alignment occurs unidirectionally rather than central dipole alignment around ions, weakening the solvation of ions. As a result, less solvated ions are more likely to form pairs, clusters, and ultimately nucleate and precipitate[15,33]. Moreover, a non-equilibrium evaporation process occurs under NTP discharge at the gas-liquid interface of the solution, causing species at the surface to be ejected into the gaseous state without requiring a large amount of thermal energy to evaporate the water[16].

3.2. Thermal profile and Optical Emission Spectroscopy (OES)

As shown in Figure 1, when a droplet starts to fall from the dripper, it initially increases in volume and then oscillates. This oscillation is likely due to the displacement of the drop's center of mass caused by the electrostatic pressure exerted on the surface charges[34]. Furthermore, NTP discharge is only generated when the droplet reaches a critical volume (as shown in Figure 1). Thus, the optical emission spectra from the ionized species observed were from the gas-liquid interface of the drop. Initially, the discharge has a lilac color, typically from ionized nitrogen species, which changes to yellow. Despite the high noise level of the baseline of the emission spectrum, a significant finding in this spectrum is the strong sodium intensity ratio at 589.5 nm (Figure 5A), which is typically due to the emission of neutral sodium atoms at the gas-liquid interface. Because of the short residence time of a droplet inside the NTP discharge region of approximately 10 ms, the emission spectra of other species, such as OH (309 nm) and Cl (725.6 nm) are not observed here, although they were observed in previous work[35].

Kang et al.[36] have also reported the emission from an electrolyte solution, and they state that sodium cations, which normally exist in aqueous solution as hydrated ions, are vaporized under NTP discharge. The aqueous sodium ions turn into a gas phase with rapid dehydration and the neutral sodium atoms are excited to the upper states of the D-line transitions by electron impact from NTP. Therefore, the discharge channels formed by NTP could also explain the rapid dehydration of ions at the gas-liquid interface, inducing nucleation and accelerating salt precipitation.

The small change in the bulk temperature estimated experimentally by thermal imaging at the NTP discharge region (Figure 5B), which is approximately 5 degrees Celsius higher than the surrounding temperature is a characteristic of NTP, where the gas temperature tends to be similar to the surrounding temperature[37]. We also measured the water temperature before and after plasma exposure using a thermometer and found no significant differences.

3.3. Chemical composition

Figure 6 shows the mass of different elements in the precipitates for both the untreated and plasma-treated solutions. Differences in elemental composition between precipitates retained on the filter after plasma treatment (T) and without treatment (U) are highlighted for samples S1 and S2. Overall, the elemental concentrations of the plasma-treated samples were proportionally higher than those of the untreated samples, except for potassium, for which the concentration was lower in sample S2 treated with plasma.

Molecular dynamics studies of the interaction of strong electric fields, 0.2 V/nm or greater, with solutions containing Cl^-, Na^+ and Pb^{2+} hydrated ions showed that hydration was significantly weakened for Pb^{2+}, while for Na^+ and Cl^-, this effect was less intense because the interaction with the second hydration shell is increased[38]. The hydration of ions also depends on the orientation of water molecules, mainly in the first hydration layer. Several authors have shown that the external electric field acts to favor hydration breakdown and the subsequent binding of dehydrated cations and anions (precipitation)[38-40].

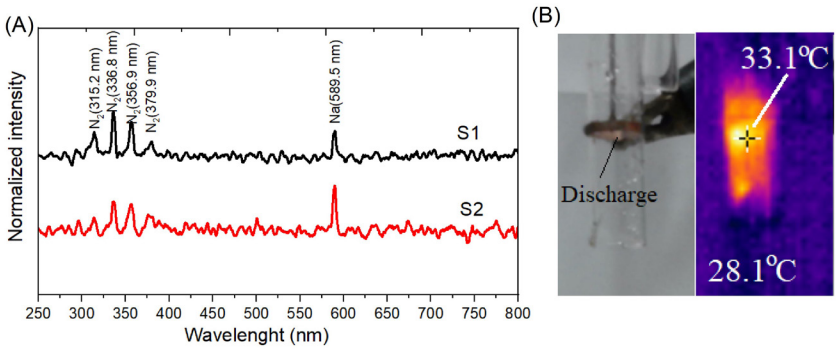

Figure 5. OES spectra of plasma species obtained during plasma treatment of droplets from samples S1 and S2 (A) and thermal profile obtained during plasma treatment (B).

To evaluate the effect of plasma on the weight per volume variation (% w/v) of each element of the precipitate, from Figure 6, we use Equation 2:

$$\%\Delta M_i = \frac{M_i^T - M_i^U}{M_i^U} x100 \quad (2)$$

where $\%\Delta M_i$ is the change in weight of element *i* in the precipitate when the solution is plasma-treated compared to the untreated solution; M_i^T is the mass of element *i* in the plasma-treated solution precipitate and M_i^U is the concentration of element *i* in the untreated-plasma solution precipitate. Table 2 presents these results. A clear relationship between the ionic species and the weakening of hydration was not identified in this analysis. However, a closer inspection of the table reveals behaviors that require further analysis. One of them is the variation in potassium concentration, which is greater after exposure to plasma in samples S1, whereas in S2 the opposite is observed. When attempting to correlate this result with the possibility of a stronger electrostatic interaction, such as the charge/valence ratio of ions, it is not possible to identify any evidence. The single most striking observation that emerged from the data comparison was that the concentration variation did not obey proportionality with the elemental concentration. The results indicate that there is preferential extraction, mainly for minor elements such as Ca^{2+}, Mg^{2+}, and SO_4^{2-} ions when the solution is treated by NTP. These results encourage the use of plasma as an energy source for the separation/extraction of salt from hypersaline waters.

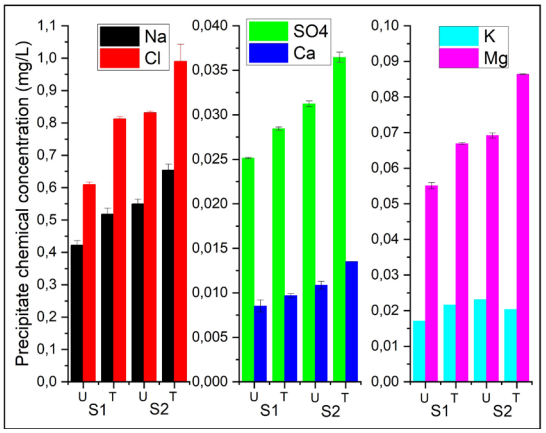

Figure 6. Chemical composition of the precipitate from untreated (U) and plasma-treated (T) solutions.

3.4 Size and morphological analysis

To observe the nucleation/crystallization of the salts, sessile drops of approximately 50 µL of each solution were collected on a glass slide and placed under a stereoscopic magnifying glass. The drops were observed with the aid of a stereoscopic magnifying glass for 50 min and then photographed (Figure 7). Crystals obtained during dripping without plasma treatment were usually cubic in morphology and sometimes orthorhombic with differences in size and distribution ranging from 600 ± 140 µm, with larger crystals closer to the drop edge (Figure 7A and 7C).

Drips under NTP treatment showed the formation of many small crystals with an average size of 360 ± 46 µm (sample S1) (Figure 7B) and 150 ± 69 µm (sample S2) (Figure 7D) compared to the untreated solution. The small crystal sizes indicate that a larger number of nucleation sites were created simultaneously under NTP treatment.

3.5. Microstructural analysis

Figure 8A shows the X-ray diffraction patterns of the precipitated salts. A halite pattern with preferential growth orientation in the (200) plane was observed, mostly in the plasma-treated samples.

A closer analysis of the peaks (Fig. 8B and 8C) shows a small angular shift with respect to the NaCl peak. These shifted peaks were identified as double salts of the MM'(SO_4) type, where M and M' are metal cations such as Na^+, K^+, Mg^{2+} or Ca^{2+}. Interestingly, the peaks of the precipitates from the plasma-treated solutions always shifted to larger angles of the crystalline structure with a minimum interplanar distance.

These microstructural changes, observed through our detailed analysis of the X-ray diffraction patterns, indicate that non-thermal plasma exposure significantly affects crystal formation mechanisms. This effect is likely due to modifications in the local chemical environment and the physical properties of the crystals, facilitated by the DBD plasma. The ability of DBD plasma to induce such modifications highlights its potential for targeted manipulation of crystallization processes in saline solutions. This capability is especially pertinent in environments where seawater composition can significantly vary, underlining the adaptability and effectiveness of plasma technology in natural settings.

Consistent with prior studies that have utilized natural seawater to evaluate the effects of non-thermal plasma on saline waters[15,16,35,41], our methodology underscores the scientific validity of using natural samples. These precedents not only bolster the robustness of our experimental design

Table 2. Weight per volume concentration variation (% w/v) of each element in the precipitate from plasma-treated compared with untreated samples.

Sample	Weight variation (% w/v)					
	Na^+	K^+	Mg^{2+}	Ca^{2+}	Cl^-	SO_4^{2-}
S1	24.0	23.5	21.8	18.8	33.0	8.8
S2	18.4	-16.7	24.6	16.1	20.4	14.3

Each value represents the average of three replicates.

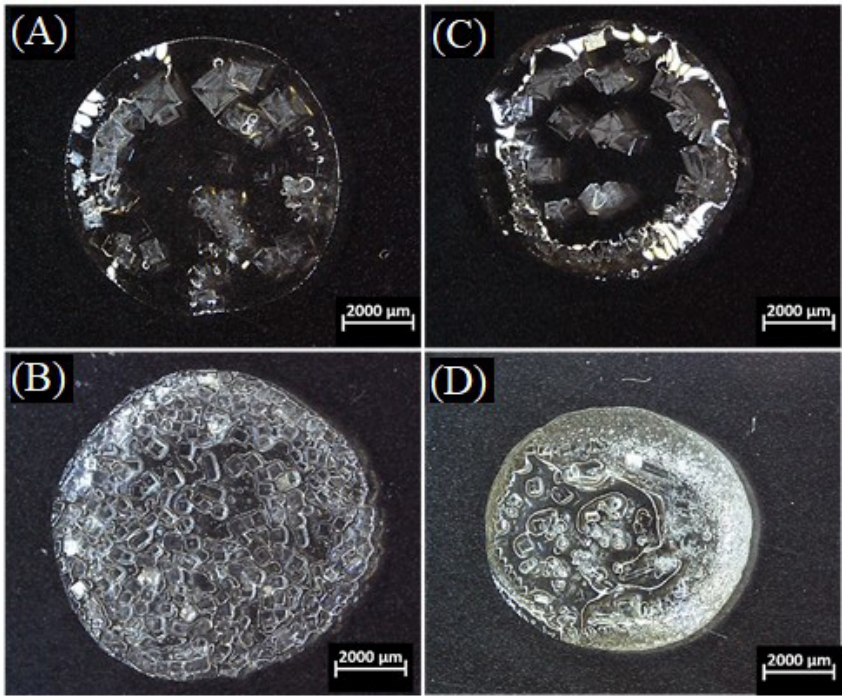

Figure 7. Photographs of the droplet surface after 50 min of drying. (A) S1 without treatment; (B) S1 after plasma treatment; (C) S2 without treatment; and (D) S2 after plasma treatment.

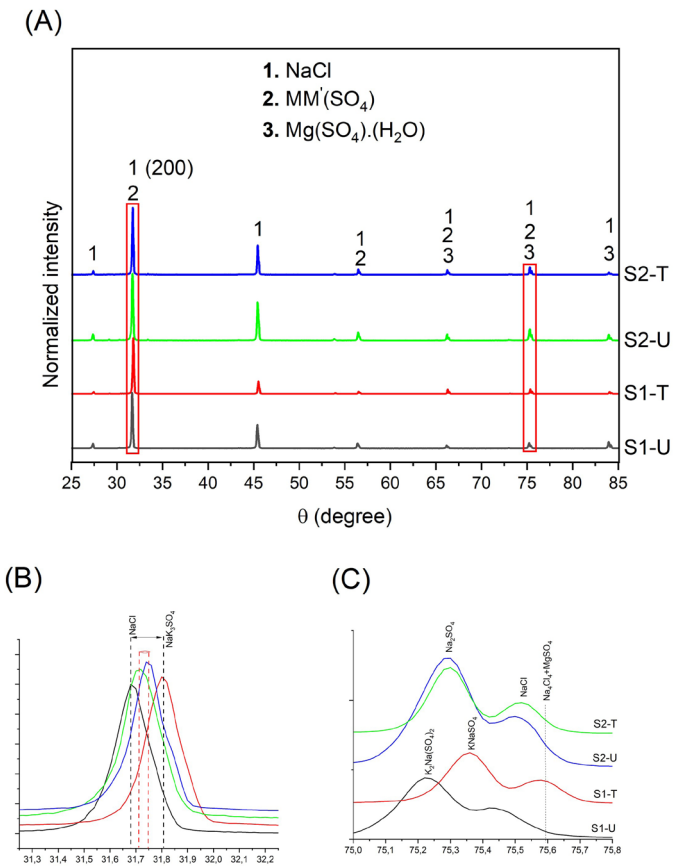

Figure 8. Diffractogram of precipitated salts obtained after dripping without (U) and with plasma treatment (T).

but also provide a solid basis for comparing the effectiveness of DBD plasma with other plasma sources. Our findings demonstrate that DBD plasma can significantly enhance natural processes such as evaporation and salt crystallization. This integration not only validates our approach but also suggests that DBD plasma could be a highly effective tool for improving industrial processes that rely on the precise control of salt precipitation and crystal morphology.

4. Conclusion

This study aimed to investigate the effects of atmospheric pressure NTP on salt precipitation in hypersaline water droplets, specifically utilizing natural seawater to replicate real industrial conditions. Our findings revealed that while NTP transferred less energy than required for salt precipitation by evaporation alone, it significantly increased the rate of salt precipitation and notably altered crystal formation mechanisms. The NTP-treated solutions exhibited a markedly higher precipitation rate, resulting in the formation of numerous small crystals. These small crystals, containing multiple charged ions, preferentially precipitated due to the external electric field generated by NTP, which aligns and weakens the hydration of ions, facilitating the binding of dehydrated cations and anions and inducing nucleation and precipitation. Furthermore, NTP formed discharge channels at the gas-liquid interface, leading to rapid dehydration of ions and further nucleation and crystal formation. This mechanism offers a compelling explanation for the preferential precipitation observed.

The use of natural seawater in our experiments underscores its critical role in studying the application of non-thermal plasma technology in salt production, echoing the conditions found in the solar salt industry. The insights gained from this study are vital for advancing practical applications in industrial settings, demonstrating the potential of NTP to enhance processes such as evaporation and salt crystallization. This study not only supports the practical use of natural seawater but also highlights its necessity in developing environmentally relevant technological solutions, making a significant contribution to the field, and offering avenues for further research and application in industrial processes.

5. Acknowledgments

This project was funded by the National Council for Scientific and Technological Development (CNPq-402536/2021-5 and 304422/2021-5), National Institute of Surface Engineering (CNPq- 465423/2014-0), and National Council for the Improvement of Higher Education (CAPES).

6. References

1. Davies PA, Knowles PR. Seawater bitterns as a source of liquid desiccant for use in solar-cooled greenhouses. Desalination. 2006;196(1-3):266-79.
2. Park K, Hong SY, Lee JW, Kang KC, Lee YC, Ha M-G, et al. A new apparatus for seawater desalination by gas hydrate process and removal characteristics of dissolved minerals (Na+, Mg2+, Ca2+, K+, B3+). Desalination. 2011;274(1-3):91-6.
3. Lopez AM, Williams M, Paiva M, Demydov D, Do TD, Fairey JL, et al. Potential of electrodialytic techniques in brackish desalination and recovery of industrial process water for reuse. Desalination. 2017;409:108-14.
4. Hussein AA, Zohdy K, Abdelkreem M. Seawater bittern a precursor for magnesium chloride separation: discussion and assessment of case studies. Int J Waste Resour. 2017;7:1-6.
5. Chen Q, Li J, Li Y. A review of plasma-liquid interactions for nanomaterial synthesis. J Phys D Appl Phys. 2015;48(42):424005.
6. Surowsky B, Schlüter O, Knorr D. Interactions of non-thermal atmospheric pressure plasma with solid and liquid food systems: a review. Food Eng Rev. 2015;7(2):82-108.
7. Rezaei F, Vanraes P, Nikiforov A, Morent R, de Geyter N. Applications of plasma-liquid systems: a review. Materials (Basel). 2019;12(17):2751.
8. Fridman A. Plasma chemistry. Cambridge: Cambridge University Press; 2008.
9. Stryczewska HD, Jakubowski T, Kalisiak S, Gizewski T, Pawlat J. Power systems of plasma reactors for non-thermal plasma generation. J Adv Oxid Technol. 2013;16(1):52-62.
10. Stratton GR, Dai F, Bellona CL, Holsen TM, Dickenson ERV, Mededovic Thagard S. Plasma-based water treatment. Environ Sci Technol. 2017;51(3):1643-8.
11. Thirumdas R, Kothakota A, Annapure U, Siliveru K, Blundell R, Gatt R, et al. Plasma activated water (PAW): Chemistry, physico-chemical properties, applications in food and agriculture. Trends Food Sci Technol. 2018;77:21-31.
12. Zarei T, Mirpour S, Nikmaram H, Ghoranneviss M, Mirpour S, Dorranian D. Softening hard water using high frequency spark plasma discharge. Plasma Chem Plasma Process. 2017;37(1):99-114.
13. Ekanayake UGM, Seo DH, Faershteyn K, O'Mullane AP, Shon H, MacLeod J, et al. Atmospheric-pressure plasma seawater desalination: clean energy, agriculture, and resource recovery nexus for a blue planet *Sustainable.* Mater Technol. 2020;25:e00181.
14. Liu ZC, Guo L, Liu DX, Rong MZ, Chen HL, Kong MG. Chemical kinetics and reactive species in normal saline activated by a surface air discharge. Plasma Process Polym. 2017;14(4-5):1600113.
15. Almada L F A, Fontes KES, Vitoriano JO, Melo VRM, Fraga FEN, Alves-Junior C. Applying pulsed corona discharge in hypersaline droplets. J Phys D Appl Phys. 2021;54(5):055202.
16. Barauna JBFO, Pereira CS, Gonçalves IA, De Oliveira Vitoriano J, Junior CA. Sodium chloride crystallization by electric discharge in brine. Mater Res. 2017;20(suppl 2):215-20.
17. Shirai N, Ichinose K, Uchida S, Tochikubo F. Influence of liquid temperature on the characteristics of an atmospheric dc glow discharge using a liquid electrode with a miniature helium flow. Plasma Sources Sci Technol. 2011;20(3):034013.
18. El-Tayeb A, El-Shazly AH, Elkady MF. Investigation the influence of different salts on the degradation of organic dyes using non-thermal plasma. Energies. 2016;9(11):874.
19. Ekanayake UGM, Barclay M, Seo DH, Park MJ, MacLeod J, O'Mullane AP, et al. Utilization of plasma in water desalination and purification. Desalination. 2021;500:114903.
20. Huang Y, Yan H, Wang B, Zhang X, Liu Z, Yan K. The electro-acoustic transition process of pulsed corona discharge in conductive water. J Phys D Appl Phys. 2014;47(25):255204.
21. Bruggeman PJ, Kushner MJ, Locke BR, Gardeniers JGE, Graham WG, Graves DB, et al. Plasma-liquid interactions: a review and roadmap. Plasma Sources Sci Technol. 2016;25(5):053002.
22. Barthakur NN. An electrostatic method of drying saline water. Dry Technol. 1989;7(3):503-21.
23. Barger JP, Dillon PF. Electrophoretic measurement of water charge density and ion hydration. Electrophoresis. 2020;41(13-14):1170-7.
24. Qu J, Escobara L, Li J, Rao Z, Xu B. Experimental study of evaporation and crystallization of brine droplets under different temperatures and humidity levels. Int. Commun. Heat Mass Transf. 2020;110:104427.

25. Kadota K, Shimosaka A, Shirakawa Y, Hidaka J. Dehydration process in NaCl solutions under various external electric fields. J Nanopart Res. 2007;9(3):377-87.
26. Bui X-T, Chiemchaisri C, Fujioka T, Varjani S. Water and wastewater treatment technologies. Singapore: Springer; 2019.
27. Oren A. Saltern evaporation ponds as model systems for the study of primary production processes under hypersaline conditions. Aquat Microb Ecol. 2009;56:193-204.
28. Shokri-Kuehni SMS, Norouzi Rad M, Webb C, Shokri N. Impact of type of salt and ambient conditions on saline water evaporation from porous media. Adv Water Resour. 2017;105:154-61.
29. Holterman HJ. Kinetics and evaporation of water drops in air. Wageningen: Instituut voor Milieu- en Agritechniek; 2003.
30. Gregson FKA, Robinson JF, Miles REH, Royall CP, Reid JP. Drying kinetics of salt solution droplets: water evaporation rates and crystallization. J Phys Chem B. 2019;123(1):266-76.
31. Yamada T, Sasagawa N, Sakai K. Accurate determination of volume and evaporation rate of micron-size liquid particle. J Appl Phys. 2010;108(6):063523.
32. Rosenthal LA, Davis DA. Electrical characterization of a corona discharge for surface treatment. IEEE Trans Ind Appl. 1975;IA-11(3):328-35.
33. Ma Y, Zhong L, Gao J, Liu L, Hu H, Yu Q. Manipulating ice crystallization of 0.9 wt.% NaCl aqueous solution by alternating current electric field. Appl Phys Lett. 2013;102(18):183701.
34. Joffre G, Prunet-Foch B, Berthomme S, Cloupeau M. Deformation of liquid menisci under the action of an electric field. J Electrost. 1982;13(2):151-65.
35. Alves-Junior C, Rodrigues-Junior FE, Vitoriano JO, Barauna JBFO. Investigating the influence of the pulsed corona discharge over hypersaline water. Mater Res. 2021;24(6):e20210261.
36. Kang WS, Hur M, Song YH. Effect of voltage polarity on the plasma-liquid interactions. Appl Phys Lett. 2015;107(9):094101.
37. Laroussi M, Lu X, Keidar M. Perspective: the physics, diagnostics, and applications of atmospheric pressure low temperature plasma sources used in plasma medicine. J Appl Phys. 2017;122(2):020901.
38. He Z, Cui H, Hao S, Wang L, Zhou J. Electric-field effects on ionic hydration: a molecular dynamics study. J Phys Chem B. 2018;122(22):5991-8.
39. Marracino P, Liberti M, Inzeo G, Apollonio F. Water response to intense electric fields : a molecular dynamics study. Bioelectromagnetics. 2015;36(5):377-85.
40. Zhu L, Han Y. Influence of alternating electric fields and impurity Mg_2^+ on $CaCl_2$ aqueous solution: a study by molecular dynamics simulation. J Mol Liq. 2018;271:820-7.
41. Emanuel Silva Fontes K, Ferreira Araújo de Almada L, Vitoriano JO, Alves C Jr. Extracting salt from hypersaline water by pulsed corona discharge. Sep Sci Technol. 2022;57(13):2065-72. http://doi.org/10.1080/01496395.2021.2017969.